Evidence that interaction between conserved residues in transmembrane helices 2, 3 and 7 are crucial for human VPAC$_1$ receptor activation.

Anton O Chugunov, John Simms, David R Poyner, Yves Dehouck, Marianne Rooman, Dimitri Gilis and Ingrid Langer

Unité de Bioinformatique génomique et structurale, Université Libre de Bruxelles, Brussels, Belgium (AC, YD, MR, DG)

M.M. Shemyakin and Yu.A. Ovchinnikov Institute of Bioorganic Chemistry, Russian Academy of Sciences, Moscow, Russia (AC)

Department of Pharmacology, University of Monash, Clayton 3800, Australia (JS)

School of Life and Health Sciences, Aston University, Birmingham, UK (DP)

IRIBHM, Université Libre de Bruxelles, Brussels, Belgium (IL)

Running title: Activation of hVPAC$_1$ receptor

Address for correspondence:

Ingrid Langer, IRIBHM, Université Libre de Bruxelles, 808 route de Lennik CP602, B-1070 Brussels, Belgium.

Phone: 32-2-5554172; Fax: 32-2-5554655

Email: ilanger@ulb.ac.be

Number of text pages: 28

Number of tables: 1

Number of figures: 4

Number of references: 38

Number of words:

      Abstract: 205

      Introduction: 478

      Discussion: 1344

Abbreviations:

3D: three dimensions; Aln: alignment; GPCR: G protein coupled receptor; MD: molecular

dynamics; MP: membrane protein; OPSD: bovine visual rhodopsin; TM: transmembrane;

VIP: vasoactive intestinal peptide.

3

ABSTRACT

The VPAC$_1$ receptor belongs to family B of G protein coupled receptors (GPCR-B) and is activated upon binding of the VIP peptide. Despite the recent solving of the structure of the N-terminus of several members of this receptor family, little is known about the structure of the transmembrane (TM) region and about the molecular mechanisms leading to activation. In the present study we designed a new structural model of the TM domain and combined it with experimental mutagenesis experiments to investigate the interaction network that governs ligand binding and receptor activation. Our results suggest that this network involves the cluster of residues R^{188} in TM2, Q^{380} in TM7 and N^{229} in TM3. This cluster is expected to be altered upon VIP binding, as R^{188} has previously been shown to interact with D^3 of VIP. Several point mutations at positions 188, 229 and 380 were experimentally characterized and shown to severely affect VIP binding and/or VIP mediated cAMP production. Double mutants built from reciprocal residue exchanges exhibit strong cooperative or anti-cooperative effects, thereby indicating the spatial proximity of residues R^{188}, Q^{380} and N^{229}. As these residues are highly conserved in the GPCR-B family, they can moreover be expected to have a general role in mediating function.

INTRODUCTION

The human $VPAC_1$ receptor is expressed in liver, breast, kidney, prostate, bladder, pancreatic ducts, thyroid gland, lymphoid tissues and gastrointestinal mucosa and in most of the tumors derived from these tissues. The $VPAC_1$ receptor is a member of family B of G protein coupled receptors (GPCR), which have seven transmembrane helices (7 TM). This family includes the $VPAC_2$-, secretin-, PAC_1-, glucagon-, glucagon like-peptide 1 and 2-, calcitonin-, corticotropin-releasing factor- and parathyroid hormone (PTH) receptors. The physiological ligands of the $VPAC_1$ receptor are Vasoactive Intestinal Polypeptide (VIP) and Pituitary Adenylate Cyclase Activating Peptide (PACAP) (Dickson and Finlayson, 2009).

Extensive studies of the largest family of GPCRs, the GPCR-A/rhodopsin family led to the identification of key steps frequently involved in the early signaling events of this family. These include the disruption of an ionic interaction between the cytoplasmic face of TM3 and TM6 maintaining the receptor preferentially in a ground inactive conformation in absence of agonist (ionic lock) and a "rotamer toggle switch" (modulation of the helix conformation around a proline-kink) in TM6 causing key sequences to be exposed to cytoplasmic binding partners (Ballesteros *et al.*, 2001;Schwartz *et al.*, 2006).

The mechanisms regulating the GPCR-B family signal transduction are less precisely understood, since no X-ray structure of the whole receptor is available, and conserved motifs of the GPCR-A family (E/DRY at TM3, NPXXY at TM7) are absent in the GPCR-B family. Although recent studies have solved the structure of the N terminus of several family B receptors (CRF, PTH, PAC_1, GIP, GLP-1) and clarified their role in ligand binding (Grace *et al.*, 2007;Parthier *et al.*, 2007;Pioszak and Xu, 2008;Runge *et al.*, 2008;Sun *et al.*, 2007), there is little information on the events that follow ligand binding. Considering the $VPAC_1$ receptor as a paradigm for class B, it actually appears that a large network of interactions must be considered. Indeed, on the basis of mutagenesis studies, it has been proposed that TM1,

TM2, TM3, and TM6, but also the intracellular loop 3 (ICL3) and the proximal part of the C-terminal intracytoplasmic tail take part in the receptor signal transduction (Gaudin *et al.*, 1998;Gaudin *et al.*, 1999;Couvineau *et al.*, 2003;Langer and Robberecht, 2007).

In the present study, a network of interactions that stabilize the VPAC$_1$ receptor conformation in absence of ligand is identified by combining modeling and mutagenesis studies, and is proposed to be involved in receptor activation. This network includes an arginine (R^{188}) located in TM2, previously demonstrated by complementary-paired mutagenesis to interact with the D^3 residue of VIP (Solano *et al.*, 2001), an asparagine (N^{229}) located in TM3, important for VPAC$_1$ and VPAC$_2$ mediated G protein activation (Nachtergael *et al.*, 2006) and a glutamine (Q^{380}) conserved among the GPCR-B family members and located in TM7. To our knowledge, this is the first identification of early steps that lead to the receptor activation of a GPCR-B family member upon ligand binding.

MATERIALS AND METHODS

Comparative modeling procedure

Comparative modeling was carried out by Modeller 9V3 (Marti-Renom *et al.*, 2000), on the basis of alignments between the target and template sequences obtained as described in Results. The modeling was constrained, in order to create an obligate disulfide bond between the residues Cys^{215} at the extracellular end of TM3 and Cys^{285} in the extracellular loop 2 (ECL2); this disulfide bridge is indeed known to occur in GPCR-B members. All models were stepwise energy-relaxed: 1) with all heavy-atoms fixed; 2) with backbone atoms fixed and 3) with C$_\alpha$ atoms fixed. Gromacs 3.3.1 was used for energy calculations (Lindahl *et al.*, 2001).

Quality assessment of the structural models

To evaluate the quality of the structural models generated from different sequence alignments, we used the membrane score approach (Chugunov *et al.*, 2007b;Chugunov *et al.*, 2007a), which was developed for the assessment of the packing quality of α-helical TM domains of membrane proteins (MP). In this method, a database-derived scoring function (S^{mem}) is used to quantitatively estimate the fitness of a given amino acid residue for its three-dimensional class of protein–membrane environment. This scoring function was derived from the analysis of a non-redundant set of α-helical MP structures (Chugunov *et al.*, 2007a). The larger S^{mem} the model has, the better it is packed in space. Generally, models with $S^{mem}<0$ should be considered as misfolded. This method has been proven to be useful in discriminating close-to-native structures from large decoy sets built from misleading alignments (Chugunov *et al.*, 2007b). A second quality assessment, performed on the best structural models identified by the membrane score approach, consisted of a detailed analysis of the variability moment vectors. In a first step, all protein sequences homologous to the target are aligned, and the amino acid variability at each position is computed. In a second step, a vector is assigned to each residue in each TM helix of the 3D model of the target. The vector is put in a plane

Molecular Pharmacology Fast Forward. Published on June 23, 2010 as DOI: 10.1124/mol.110.063578

MOL #63578 This article has not been copyedited and formatted. The final version may differ from this version.   7

parallel to the surface of the membrane, points out of the helix, and its amplitude is proportional to the variability of the residue among the members of the target family. The resulting vector is computed for each helix, and shows thus the most variable side of the helix, which should be exposed to the membrane, since evolution is known to better conserve amino acids that point towards the protein core and are likely to be involved in important interactions. The models that fulfill the previous quality assessments were submitted to a 1 ns molecular dynamics (MD) simulation in vacuum at 500 K, with fixed C_α atoms solely for exploration of side chains motility (not for model optimization). GROMACS 3.3.1 (Lindahl *et al.*, 2001) was used for that purpose. More sophisticated MD calculations would require an explicitly defined medium (membrane) and advanced setup, but for our purposes, the sampling of the side chain conformations with a fixed backbone is sufficient. During each MD simulation, 1000 frames were memorized, and the S^{mem} values were computed for each of them to cumulate score distributions.

Construction and expression of VPAC$_1$ mutant receptors

The cell lines expressing wild-type (wt) VPAC$_1$, as well as $R^{188}A$, $R^{188}Q$, $N^{229}A$ and $N^{229}Q$ mutant receptors, have been detailed in previous publications (Nachtergael *et al.*, 2006;Solano *et al.*, 2001). The generation of the other mutated receptors was achieved using the QuikChange Site-Directed Mutagenesis kit (Stratagene, LaJolla CA, USA), according to the manufacturer's instructions. Confirmation of the expected mutation was achieved by DNA sequencing on an ABI automated sequencing apparatus, using the BigDye Terminator Sequencing Prism Kit from ABI (Perkin-Elmer, CA, USA). Following DNA amplification using a midiprep endotoxin-free kit (Promega, CA, USA), the complete nucleotide sequence of the receptor coding region was verified by DNA sequencing. 20 µg of DNA was transfected by electroporation in CHO cell line expressing aequorin (kindly provided by Vincent Dupriez, Euroscreen SA, Belgium) as described in (Nachtergael *et al.*, 2006).

Selection was carried out in the culture medium [50% HamF12; 50% DMEM; 10% Fetal Calf Serum; 1% Penicillin (10 mU/ml); 1% Streptomycin (10 µg/ml); 1% L-Glutamine (200 mM), PAA, Pashing, Austria], supplemented with 600 µg Geneticin (G418)/ml culture medium. After 10 to 15 days of selection, isolated colonies were transferred to 24 well plates and grown until confluence, trypsinized and further expanded in 6 well plates, from which cells were scraped and membranes prepared for identification of receptor expressing clones by an adenylate cyclase activity assay in presence of 1 µM VIP and by binding assay with [125I]-VIP (see below).

Membrane preparation

Membranes were prepared from scraped cells lysed in 1 mM NaHCO3 followed by immediate freezing in liquid nitrogen. After thawing, the lysate was first centrifuged at 4°C for 10 min at 400 g and the supernatant was further centrifuged at 20 000 g for 10 min. The resulting pellet, resuspended in 1 mM NaHCO3 was used immediately as a crude membrane fraction.

Adenylate cyclase activation assay

Adenylate cyclase activity was determined by the procedure described (Salomon *et al.*, 1974). Membrane proteins (3-15 µg) were incubated in a total volume of 60 µl containing 0.5 mM [α^{32}P]-ATP, 10 µM GTP, 5 mM MgCl$_2$, 0.5 mM EGTA, 1 mM cAMP, 1 mM theophylline, 10 mM phospho(enol)pyruvate, 30 µg/ml pyruvate kinase and 30 mM Tris-HCl at a final pH of 7.8. The reaction was initiated by membranes addition and was terminated after 15 min incubation at 37°C by adding 0.5 ml of a 0.5 % sodium dodecyl-sulfate solution containing 0.5 mM ATP, 0.5 mM cAMP and 20000 cpm [^{3}H]-cAMP. cAMP was separated from ATP by two successive chromatographies on Dowex 50W x 8 and neutral alumina.

Binding studies

This article has not been copyedited and formatted. The final version may differ from this version.   9

Binding studies on $VPAC_1$ wt and mutant receptors were performed by using the $[^{125}I]$-VIP. The non specific binding was defined as residual binding in the presence of 1 µM unlabeled VIP. Binding was performed for 30 min at 23°C in a total volume of 120 µl containing 20 mM Tris-maleate, 2 mM $MgCl_2$, 0.1 mg/ml bacitracin, 1% bovine serum albumin (pH 7.4) buffer using 3 to 30 µg of protein per assay. Bound and free radioactivity were separated by filtration through glass-fiber GF/C filters presoaked for 24 h in 0.01% polyethyleneimine and rinsed three times with a 20 mM (pH 7.4) sodium phosphate buffer containing 0.8 % bovine serum albumin. The binding sites density was estimated by analysis of homologous competition curves assuming that the labelled and unlabeled ligands had the same affinity for the receptors.

Peptide synthesis

The peptides used were synthesized in our laboratory as described in (Nachtergael *et al.*, 2006). Peptide purity (at least 95%) was assessed by capillary electrophoresis, and conformity by electrospray MS.

Data analysis

All competition curves, dose-response curves, pIC_{50} and pEC_{50} values were calculated using non linear regression (GraphPad Prism software). Statistical analyses were performed with the same software.

RESULTS

Molecular modeling

Since no experimental VPAC$_1$ structure is available, molecular modeling of its TM domain was performed in view of identifying residues involved in VIP binding and receptor activation, selecting potentially interesting mutations to be studied experimentally and rationalizing the results of these analyses. We took advantage of a preliminary 3D model of the TM domain of VPAC$_1$ (Conner *et al.*, 2005) and designed a new, carefully optimized, model.

An important ingredient towards optimal modeling is the production of a correct amino acid alignment between the template and target proteins, given the almost non-significant level of sequence identity between the members of the GPCR-B family and the GPCR-A receptors for which several structures have been solved (Palczewski *et al.*, 2000;Okada *et al.*, 2004;Cherezov *et al.*, 2007;Warne *et al.*, 2008;Jaakola *et al.*, 2008). There is moreover no evidence that the receptors' activation mechanism should be the same in GPCR-A and GPCR-B, and involve similar intermediate states. So, there is no clear reason of selecting any particular structural template for modeling GPCR-B proteins. Here we chose the well-resolved crystallographic structure of bovine visual rhodopsin (PDB code: 1U19) (Okada *et al.*, 2004).

Sequence alignments and TM model

Since commonly available and automatic sequence alignment methods fail to produce reliable OPSD–VPAC$_1$ alignments due to their very low sequence identity, we turned to an iterative and partly manual procedure of sequence alignment selection.

In a first step, we compiled a set of four OPSD–VPAC$_1$ alignments (Aln-1 to Aln-4). Aln-1 was adapted from the approach of Frimurer & Bywater for the modeling of the GLP-1

Molecular Pharmacology Fast Forward. Published on June 23, 2010 as DOI: 10.1124/mol.110.063578

MOL #63578 article has not been copyedited and formatted. The final version may differ from this version.   11

receptor based on a comprehensive sequence analysis, a low-resolution structure of frog rhodopsin obtained by electron crystallography, and the so-called "cold-spot" alignment method for sequences with low similarity (Frimurer and Bywater, 1999) Aln-2 was taken from the work of Bisstantz *et al.* (Bissantz *et al.*, 2004), in which they defined a framework for the automated modeling of GPCRs of the three main subfamilies. The latter approach tends to superimpose highly conserved positions, irrespective of their physicochemical nature, rather than residues viewed as similar according to substitution matrices. Aln-3 was built manually, by implementing a kind of "cold-spot" approach idea. No gaps were allowed inside the TM domain; they were moved to the middle of loop regions. Aln-4 was produced by mGenThreader (McGuffin *et al.*, 2000) *via* the BioInfoBank Meta Server (Ginalski *et al.*, 2003).All these alignments along with final variant can be found in Figure S1.

The four alignments were in agreement for helices TM3, TM6 and TM7, but they differed considerably for the other ones: we obtained 4, 2, 2, and 3 variants for TM1, TM2, TM4 and TM5, respectively. Considering the sequence as a whole, this corresponds to 48 ($4\times2\times2\times3$) global alignment variants of the TM region.

Each of the 48 alignments so obtained was used to generate a set of ten structural models, using the comparative modeling approach described in Methods. The packing quality of the TM helices in these 480 models was assessed using the membrane score S^{mem} (see Methods). In a second step, the alignment that produced the best structural models, which display the maximum S^{mem} value averaged over the 10 models ($< S^{mem} >$), was used as starting point for further exploration of the alignment space This involved generating $3^7=2187$ alignment variants by shifting each of the 7 TM helices independently by -1, 0, or $+1$ residue. From each of these new alignments, 10 structural models were built and evaluated on the basis of the membrane score S^{mem}. The best alignment at this stage, referred to as ReAln (see Fig. S1), was submitted again to the same helix shifting procedure, leading to 2187 other alignment

variants. However, the models produced from these new alignments are not superior to that from ReAln (data not shown). The procedure was therefore stopped, and ReAln was considered to be the optimal alignment as measured by the S^{mem} score.

Given the shortcomings of the empirical membrane score method, it is essential to consider available data on homologous proteins and check whether the model meets the general packing principles for membrane proteins such as hydrophobicity and variability organization. In particular, it is well known that the side of a given secondary structure element (here, an α-helix) that has mutated most during evolution is always exposed to the surrounding medium (here, the membrane). On the contrary, the conserved side, which is likely to play some important structural or functional roles, is buried inside the protein interior (Beuming and Weinstein, 2004). We performed thus a detailed analysis of the variability moment vectors in the structural model (see experimental procedures and Figure S2), and corrected manually the ReAln alignment to fulfill the requirement that the most variable side of the helix should face the membrane. The final alignment, which we refer to as finalAln, is given in Fig. 1 (see also Fig. S1).

Despite a better variability and hydrophobicity organization, the models based on the final alignment finalAln (Fig. 1) demonstrated seriously impaired S^{mem} values in comparison with the ReAln-based models. This may be the consequence of a known caveat of the membrane score method, *i.e.* an excessive sensitivity to small conformational changes of the amino acids' side chains. To analyze whether these bad S^{mem} values are indeed due to not accounting for the flexible nature of protein side chains, we performed molecular dynamics (MD) runs with a fixed backbone conformation and computed the S^{mem} values along the MD trajectories, as described in Methods. The comparison of the resulting S^{mem} distributions (Fig. 2) shows that the final alignment finalAln generally leads to better packed models than the ReAln alignment, even though the starting conformations of the MD simulation present a lower S^{mem}

Molecular Pharmacology Fast Forward. Published on June 23, 2010 as DOI: 10.1124/mol.110.063578

MOL #63578 This article has not been copyedited and formatted. The final version may differ from this version.   13

score in the case of finalAln than for ReAln. Note that the four initial alignments (Aln-1–4), which came from a single source and not from an iterative semi-manual alignment procedure (Fig. S1), exhibit much worse S^{mem} distributions than ReAln and finalAln (Fig. 2). We thus definitely consider finalAln as the optimal alignment and the resulting 3D models as the optimal model structures.

Analysis of the TM model

The resulting model of $VPAC_1$ TM domain, depicted in Fig. 3, has native-like variability (Fig. S2) and hydrophobicity organization (data not shown). In addition, all residues that are known to be functionally important are located in an environment that provides a reasonable explanation of their function. The only polar stretch in contact with the membrane is located on the TM4 surface (Figure S3), which has been experimentally shown to correspond to a dimerization site in the case of the secretin receptor (Harikumar *et al.*, 2007). This site may thus be expected to correspond to a dimerization site for the $VPAC_1$ receptor too.

As seen in Figure 3, residues that are known to mediate ligand binding — R^{188}, K^{195} and D^{196} in TM2 (Solano *et al.*, 2001;Langer and Robberecht, 2007) — form a cavity close to the exterior surface of the membrane, with the charged group of R^{188} at the very bottom of the cavity. An interhelical interaction R^{188}–Q^{380} between TM2 and TM7, analogous to the R^{233}–Q^{451} interaction shown to be important for PTHR1 receptor (Gardella *et al.*, 1996), is moreover observed in the model. This interaction can partially compensate for the unfavorable presence of the positive charge of R^{188} inside the helix bundle in absence of ligand. These two residues belong to a chain of polar residues inside the receptor bundle: R^{188} in TM2 – Q^{380} in TM7 – N^{229} in TM3 (Figure 3c). H^{178} in TM2 and T^{343} in TM6, described as important for the activation and constitutive activity of some family B receptors (Hjorth *et al.*, 1998;Gaudin *et al.*, 1999), are as well incorporated in a polar network in the cytoplasmic half of the TM domain of the receptor.

Experimental analyses

Q^{380} located in TM7 is important for $VPAC_1$ activation

Mutagenesis and functional studies previously identified an asparagine located in TM3 (N^{229} and N^{216} in $VPAC_1$ and $VPAC_2$ receptor respectively) that is essential for receptor activation (Nachtergael *et al.*, 2006). Indeed, as reported in Table 1, the $N^{229}A$ and $N^{229}Q$ mutations were shown to reduce the potency to stimulate adenylate cyclase by 10 fold. Furthermore, R^{188} in TM2 was previously demonstrated to establish a salt bridge interaction with D^3 of VIP, which is essential for $VPAC_1$ activation (Solano *et al.*, 2001). Indeed, the $R^{188}A$ and $R^{188}Q$ mutations drastically impair both VIP binding and adenylate cyclase stimulation (Table 1), whereas the double mutant $R^{188}Q$ in $VPAC_1$ and D^3N in VIP is fully functional. These results led us to postulate that both N^{229} and R^{188} residues could be involved in an interaction network between TM helices, stabilizing the active receptor conformation, as often observed in GPCR-A family receptors.

To identify other residues likely to take part in the network, we took advantage of the 3D model presented here above and searched for amino acids located in vicinity of N^{229} and R^{188}. As shown in Figure 3, the ideal candidate is Q^{380} in TM7, which appears to be sandwiched between N^{229} and R^{188}. To evaluate the potential role of Q^{380}, we substituted this residue into Ala, Arg or Asn and performed binding competition curves as well as dose response curves of adenylate cyclase stimulation. As shown in Table 1 and Figure 4, the $Q^{380}A$ and $Q^{380}N$ mutants preserve the affinity for VIP, whereas $Q^{380}R$ shows a 20-fold decrease in affinity ($\Delta pIC_{50}= -1.35$). The 3 mutants moreover display a decrease in the maximal cyclic AMP stimulation for a comparable receptor density, and a decrease in the pEC_{50} value of adenylate cyclase activation. This effect is stronger for $Q^{380}A$ and $Q^{380}R$ and relatively weak for $Q^{380}N$. These results indicate that Q^{380} is important for $VPAC_1$ activation, but probably not directly

Molecular Pharmacology Fast Forward. Published on June 23, 2010 as DOI: 10.1124/mol.110.063578

MOL #63578 This article has not been copyedited and formatted. The final version may differ from this version.　　15

involved in VIP binding. Note that the reason why $Q^{380}R$ displays a decreased affinity for VIP is probably related to the proximity of R^{188} and the repulsion between positive charges.

Effect of double mutations of R^{188}, N^{229} and Q^{380}

To evaluate whether R^{188}, N^{229} and Q^{380} are functionally interdependent, as proposed by the model, we next introduced in $VPAC_1$ double mutations and compared the results with the effects obtained with the corresponding single mutants. Indeed, functionally independent residues should exhibit additive effects, while some synergy, either positive or negative may appear for functionally interdependent residues. We thus constructed mutant receptors containing double substitutions of the three residues of interest as well as the double mutation where both N^{229} and Q^{380} are replaced by an alanine. Note that we did not test double mutants containing mutation of R^{188} into alanine as the $R^{188}A$ mutant was so much affected that we were unable to characterize it (Solano *et al.*, 2001). Cell surface expression of all mutants tested was evaluated by FACS analysis using specific monoclonal anti-$VPAC_1$ antibody to ensure that the effect observed is not due to receptor misfolding or altered cell surface targeting (data not shown).

As shown in Table 1, the capability to stimulate adenylate cyclase activity of the $N^{229}A/Q^{380}A$ mutant is lower than that of the wt and similar to that of the individual single-site mutants. Furthermore, the double substitution $N^{229}Q/Q^{380}N$ only slightly reduces VIP potency and efficacy to activate adenylate cyclase and displayed a pharmacological profile intermediary between the $N^{229}Q$ and the $Q^{380}N$ mutants (Figure 4). The $Q^{380}N$ mutation thus partly restores the loss of activity caused by the $N^{229}Q$ mutation. These results tend to confirm the model, in particular the proximity of N^{229} and Q^{380}, and the importance of their interaction for $VPAC_1$ activation. Note that both double mutants present some decreased affinity for VIP, whereas no such effect is observed for the single mutants. This may result from packing defects that

indirectly affect the surrounding ligand-binding residues. This is consistent with the larger decrease in affinity caused by $N^{229}A/Q^{380}A$, as compared to $N^{229}Q/Q^{380}N$.

The double substitution $R^{188}N/N^{229}R$ resulted in a marked synergistic effect on the decrease in binding as compared to $R^{188}N$ and $N^{229}R$ mutants. Indeed we were unable to detect any VIP specific binding for the $R^{188}N/N^{229}R$ mutant, suggesting that VIP affinity is much more affected than for $R^{188}N$ mutant despite the fact that it was preserved for the $N^{229}R$ mutant. Similarly, VIP potency to stimulate adenylate cyclase was reduced by 100 fold for the $R^{188}N/N^{229}R$ mutant, by 10 fold for $R^{188}N$ but was preserved for $N^{229}R$; the VIP efficacy was reduced by 25% for both $R^{188}N/N^{229}R$ and $N^{229}R$ mutants (Table 1 and Figure 4).

Moreover, $R^{188}Q/Q^{380}R$ showed synergy in reducing the potency of VIP on cAMP production and a less-than-additive effect on binding as compared to $R^{188}Q$ and $Q^{380}R$ mutants. Indeed, VIP affinity was reduced by 100, 20 and 100 fold for $R^{188}Q$, $Q^{380}R$ and $R^{188}Q/Q^{380}R$ mutants respectively. VIP potency to stimulate adenylate cyclase was reduced by 7- and 6-fold for $R^{188}Q$ and $Q^{380}R$ mutants respectively but by 150-fold for the $R^{188}Q/Q^{380}R$ mutant. VIP efficacy was dramatically impaired for the $Q^{380}R$ and $R^{188}Q/Q^{380}R$ mutants but preserved for the $R^{188}Q$ mutant (Table 1 and Figure 4).

Altogether these data suggest that R^{188}, N^{229} and Q^{380} are functionally interdependent and important for both VIP affinity and VPAC$_1$ activation.

DISCUSSION

G protein coupled receptors, also referred to as seven transmembrane domain receptors, represent the largest family of signal transducers for extracellular stimuli. The recent solving of the high resolution structure of members of family A of GPCRs (Palczewski *et al.*, 2000;Okada *et al.*, 2004;Cherezov *et al.*, 2007;Warne *et al.*, 2008;Jaakola *et al.*, 2008) confirmed that receptor activation is mediated by relative movements among the seven transmembrane helices that are stabilized by different network of interactions. However, as these key residues are not conserved in family B GPCRs, and structural data are only available for the N-terminal extracellular domain, little is known about the precise mechanisms involved in the activation of this family of receptors.

The commonly accepted model for agonist action uses the PTH receptor as template, and suggests that the N-terminal domain is the principal binding site for the C-terminal region of the exogenous ligand, whereas binding of residues 1-3 of the ligand to the extracellular loops and TM helices are thought to drive the receptor activation and subsequent G protein coupling. Following agonist binding, subsequent conformational changes are expected within the TM domain of the receptor. This is illustrated by the fact that a Zn(II) bridge between helices 3 and 6 of the PTH receptor constrains the receptor in a conformation unable to promote PTH-mediated G-protein activation while agonist induced internalization or phosphorylation were preserved (Castro *et al.*, 2005;Vilardaga *et al.*, 2001).

In the present study, by combining pharmacological and *in silico* approaches, we have identified a network of interactions between residues located in helices 2, 3 and 7 of the VPAC$_1$ receptor, which are involved in the stabilization of the receptor in absence of agonist and in early steps of receptor activation. We propose that, in absence of VIP, the Q^{380} residue of TM7 interacts with R^{188}, located in TM2 and previously identified as essential for recognition of the D^3 side chain of VIP and subsequent receptor activation. Upon VIP binding

the interaction between R^{188} and Q^{380} is broken and a stronger interaction (salt bridge) is established between R^{188} and the D^3 side chain of VIP. This necessarily has an impact on the network of interactions essential for G protein activation, in which Q^{380} and N^{229} are proposed to play an important role. This view is supported by several experimental and modeling results.

First, we showed that the substitution of Q^{380} to alanine or asparagine significantly reduced the VIP efficacy to stimulate adenylate activation, similarly to what happens for the N^{229} substitutions (Nachtergael *et al.*, 2006), and that the substitution of both residues to Ala had a less than additive effect. The altered activation observed with these mutants cannot be attributed to the disruption of the binding pocket because the affinities for VIP were not affected for $N^{229}A$, $N^{229}Q$, $Q^{380}A$ and $Q^{380}N$ mutants. As previously suggested for N^{229}, it is likely that $Q^{380}A$ and $Q^{380}N$ mutants still bind the G protein but fail to activate it properly. As shown for several GPCRs, it is expected that reciprocal exchange of two residues involved in a direct interaction should restore the activity of the receptor. We found that the $N^{299}Q/Q^{380}N$ substitution partially restored the receptor activity. The $N^{299}A/Q^{380}A$ shows a similar anti-cooperativity since the loss in activity of the double mutant is only slightly larger than that of each single-site mutation. Note that both double mutants present a loss in binding affinity, which contributes to the loss in activity. As a consequence, the actual anti-cooperative effect is even stronger than suggested by the comparison of the measured and expected ΔpEC_{50} values (Table 1b). Thus altogether the results suggest that the interaction between N^{229} and Q^{380} is important for $VPAC_1$ mediated G protein activation.

The 3D model can be taken to suggest that Q^{380} functions as a floating "ferry-boat", switching between R^{188} and N^{229} residues' side-chains. This triad lines up in the model almost perfectly (Figure 3c), so disruption of the R^{188}–Q^{380} interaction upon VIP binding probably modifies the N^{229}–Q^{380} interaction, hence contributing to signal transduction propagation and activation

Molecular Pharmacology Fast Forward. Published on June 23, 2010 as DOI: 10.1124/mol.110.063578

MOL #63578 This article has not been copyedited and formatted. The final version may differ from this version.   19

of G protein. However, the exact mechanism by which this occurs cannot be determined at this stage, because this would require a model of the activated receptor in complex with VIP. In particular the two N-terminal residues of VIP, H^1 and S^2, are likely to affect, directly or indirectly, the interaction network surrounding N^{229} and Q^{380}.

It is also interesting to note that none of the tested single-site mutations of N^{229} or Q^{380} affects the affinity for VIP, except $Q^{380}R$. This exception can be explained by the proximity in the mutant of two arginine residues at position 188 and 380, which will create repulsive interactions modifying the relative position of the two side chains as compared to the wt receptor. These results indicate that N^{229} or Q^{380} are probably not directly involved in VIP binding.

Reciprocal substitution mutants are in agreement with the importance of R^{188} for the high affinity binding of VIP. Indeed, no specific VIP binding was detected for the $R^{188}N/N^{229}R$ mutant and VIP affinity was reduced by 150 fold for $R^{188}Q/Q^{380}R$. In those mutants, the localization of the arginine could actually be much deeper into the helices, thus preventing interaction with the D^3 side chain of VIP.

To our knowledge, this is the first study that identified, in a member of family B GPCRs, interactions between residues located in transmembrane helices that are involved in the stabilization of the receptor conformation. Interestingly, R^{172} in the closely related $VPAC_2$ receptor and R^{166} in the secretin receptor (these positions correspond to R^{188} in $VPAC_1$) also interact with the D^3 side chain of VIP and secretin, respectively (Di Paolo *et al.*, 1998;Langer and Robberecht, 2007). Some of us also previously demonstrated that N^{216} in $VPAC_2$, corresponding to N^{229} in $VPAC_1$, was essential for receptor activation (Nachtergael *et al.*, 2006). Similarly, other studies have pointed out the importance of TM2 and TM7 in G protein activation. Indeed, the mutation of H^{178} into R located at the bottom of TM2 in $VPAC_1$ led to a constitutively activated receptor (Gaudin *et al.*, 1998). As the mutation of this residue into

A, D or even K did not confer ligand-independent activation, the authors proposed that the replacement by an arginine provokes subtle conformational changes that do not simply remove some stabilizing interactions, as seen in family A GPCRs (Gaudin *et al.*, 1998). On the other hand, it has also been shown that E^{394} located at the junction of TM7 and the C-terminus of $VPAC_1$ was important for G protein activation but not for coupling (Couvineau *et al.*, 2003).

In agreement with these data and on the basis of the present results, we propose that, in absence of ligand, interaction between R^{188}, N^{229} and Q^{380} ties helices 2, 3 and 7 together. As there is no evidence for increased constitutive activity with any mutants studied, this suggests that the wild-type network of interactions is not the unique determinant for maintaining the receptor in its inactive conformation in absence of ligand. Alternatively, it is possible that multiple interactions constrain the receptor in an inactive conformation and just disrupting one doesn't lead to enhanced basal activity. Upon interaction of the N-terminal tail of VIP with the TM domain of $VPAC_1$, which includes the D^3(VIP)–R^{188}($VPAC_1$) salt bridge, TM2 and probably other helices undergo conformational modulations causing key sequences located in intracellular loops to be exposed and to interact with the G protein. In the meantime, the interaction network involving N^{229} and Q^{380} maintains TM7 in a conformation necessary for proper activation of G protein, mediated through interaction with E^{394}.

Note that the importance of R^{188}, N^{229}, Q^{380} and E^{394} residues in $VPAC_1$ activity is further supported by their high degree of conservation among all members of GPCR-B family (See Fig. S4 in supplementary material for sequence alignment of TM2, 3 and 7 of GPCR-B family members). These residues may therefore be involved in a binding and activation mechanism that is common to the whole GPCR-B family. However, additional experiments on other family members should be performed to support this view.

Molecular Pharmacology Fast Forward. Published on June 23, 2010 as DOI: 10.1124/mol.110.063578

MOL #63578 This article has not been copyedited and formatted. The final version may differ from this version. 21

ACKNOWLEDGMENTS

REFERENCES

Baker D and Sali A (2001) Protein Structure Prediction and Structural Genomics. *Science* **294**: 93-96.

Ballesteros JA, Jensen A D, Liapakis G, Rasmussen S G, Shi L, Gether U and Javitch J A (2001) Activation of the Beta 2-Adrenergic Receptor Involves Disruption of an Ionic Lock Between the Cytoplasmic Ends of Transmembrane Segments 3 and 6. *J Biol Chem* **276**: 29171-29177.

Ballesteros JA and Weinstein H (2005) Integrated Methods for the Construction of Three-Dimensional Models and Computational Probing of Structure-Function Relations in G Protein-Coupled Receptors. *Methods Neurosci* **25**: 366-428.

Beuming T and Weinstein H (2004) A Knowledge-Based Scale for the Analysis and Prediction of Buried and Exposed Faces of Transmembrane Domain Proteins. *Bioinformatics* **20**: 1822-1835.

Bissantz C, Logean A and Rognan D (2004) High-Throughput Modeling of Human G-Protein Coupled Receptors: Amino Acid Sequence Alignment, Three-Dimensional Model Building, and Receptor Library Screening. *J Chem Inf Comput Sci* **44**: 1162-1176.

Castro M, Nikolaev V O, Palm D, Lohse M J and Vilardaga J P (2005) Turn-on Switch in Parathyroid Hormone Receptor by a Two-Step Parathyroid Hormone Binding Mechanism. *Proc Natl Acad Sci U S A* **102**: 16084-16089.

Cherezov V, Rosenbaum D M, Hanson M A, Rasmussen S G, Thian F S, Kobilka T S, Choi H J, Kuhn P, Weis W I, Kobilka B K and Stevens R C (2007) High-Resolution Crystal Structure of an Engineered Human Beta2-Adrenergic G Protein-Coupled Receptor. *Science* **318**: 1258-1265.

Chugunov AO, Novoseletsky V N, Nolde D E, Arseniev A S and Efremov R G (2007a) Method to Assess Packing Quality of Transmembrane Alpha-Helices in Proteins. 1. Parametrization Using Structural Data. *J Chem Inf Model* **47**: 1150-1162.

Chugunov AO, Novoseletsky V N, Nolde D E, Arseniev A S and Efremov R G (2007b) Method to Assess Packing Quality of Transmembrane Alpha-Helices in Proteins. 2. Validation by "Correct Vs Misleading" Test. *J Chem Inf Model* **47**: 1163-1170.

Conner AC, Hay D L, Simms J, Howitt S G, Schindler M, Smith D M, Wheatley M and Poyner D R (2005) A Key Role for Transmembrane Prolines in Calcitonin Receptor-Like Receptor Agonist Binding and Signalling: Implications for Family B G-Protein-Coupled Receptors. *Mol Pharmacol* **67**: 20-31.

Couvineau A, Lacapere J J, Tan Y V, Rouyer-Fessard C, Nicole P and Laburthe M (2003) Identification of Cytoplasmic Domains of HVPAC1 Receptor Required for Activation of Adenylyl Cyclase. Crucial Role of Two Charged Amino Acids Strictly Conserved in Class II G Protein-Coupled Receptors. *J Biol Chem* **278**: 24759-24766.

Di Paolo E, De Neef P, Moguilevsky N, Petry H, Bollen A, Waelbroeck M and Robberecht P (1998) Contribution of the Second Transmembrane Helix of the Secretin Receptor to the Positioning of Secretin. *FEBS Lett* **424**: 207-210.

Dickson L and Finlayson K (2009) VPAC and PAC Receptors: From Ligands to Function. *Pharmacol Ther* **121**: 294-316.

Frimurer TM and Bywater R P (1999) Structure of the Integral Membrane Domain of the GLP1 Receptor. *Proteins* **35**: 375-386.

Gardella TJ, Luck M D, Fan M H and Lee C (1996) Transmembrane Residues of the Parathyroid Hormone (PTH)/PTH-Related Peptide Receptor That Specifically Affect Binding and Signaling by Agonist Ligands. *J Biol Chem* **271**: 12820-12825.

Gaudin P, Couvineau A, Rouyer-Fessard C, Maoret J J and Laburthe M (1999) The Human Vasoactive Intestinal Peptide/Pituitary Adenylate Cyclase Activating Peptide Receptor 1 (VPAC1): Constitutive Activation by Mutations at Threonine 343. *Biochem Biophys Res Commun* **254**: 15-20.

Gaudin P, Maoret J J, Couvineau A, Rouyer-Fessard C and Laburthe M (1998) Constitutive Activation of the Human Vasoactive Intestinal Peptide 1 Receptor, a Member of the New Class II Family of G Protein-Coupled Receptors. *J Biol Chem* **273**: 4990-4996.

Ginalski K, Elofsson A, Fischer D and Rychlewski L (2003) 3D-Jury: a Simple Approach to Improve Protein Structure Predictions. *Bioinformatics* **19**: 1015-1018.

Grace CR, Perrin M H, Gulyas J, Digruccio M R, Cantle J P, Rivier J E, Vale W W and Riek R (2007) Structure of the N-Terminal Domain of a Type B1 G Protein-Coupled Receptor in Complex With a Peptide Ligand. *Proc Natl Acad Sci U S A* **104**: 4858-4863.

Harikumar KG, Pinon D I and Miller L J (2007) Transmembrane Segment IV Contributes a Functionally Important Interface for Oligomerization of the Class II G Protein-Coupled Secretin Receptor. *J Biol Chem* **282**: 30363-30372.

Hjorth SA, Orskov C and Schwartz T W (1998) Constitutive Activity of Glucagon Receptor Mutants. *Mol Endocrinol* **12**: 78-86.

Jaakola VP, Griffith M T, Hanson M A, Cherezov V, Chien E Y, Lane J R, Ijzerman A P and Stevens R C (2008) The 2.6 Angstrom Crystal Structure of a Human A2A Adenosine Receptor Bound to an Antagonist. *Science* **322**: 1211-1217.

Langer I and Robberecht P (2007) Molecular Mechanisms Involved in Vasoactive Intestinal Peptide Receptor Activation and Regulation: Current Knowledge, Similarities to and Differences From the A Family of G-Protein-Coupled Receptors. *Biochem Soc Trans* **35**: 724-728.

Lindahl E, Hess B and van der Spoel D (2001) GROMACS 3.0: A Package for Molecular Simulationand Trajectory Analysis. *J Mol Med* **7**: 306-317.

Marti-Renom MA, Stuart A C, Fiser A, Sanchez R, Melo F and Sali A (2000) Comparative Protein Structure Modeling of Genes and Genomes. *Annu Rev Biophys Biomol Struct* **29**: 291-325.

McGuffin LJ, Bryson K and Jones D T (2000) The PSIPRED Protein Structure Prediction Server. *Bioinformatics* **16**: 404-405.

Nachtergael I, Gaspard N, Langlet C, Robberecht P and Langer I (2006) Asn229 in the Third Helix of VPAC1 Receptor Is Essential for Receptor Activation but Not for Receptor Phosphorylation and Internalization: Comparison With Asn216 in VPAC2 Receptor. *Cell Signal* **18**: 2121-2130.

Okada T, Sugihara M, Bondar A N, Elstner M, Entel P and Buss V (2004) The Retinal Conformation and Its Environment in Rhodopsin in Light of a New 2.2 A Crystal Structure. *J Mol Biol* **342**: 571-583.

Palczewski K, Kumasaka T, Hori T, Behnke C A, Motoshima H, Fox B A, Le T, I, Teller D C, Okada T, Stenkamp R E, Yamamoto M and Miyano M (2000) Crystal Structure of Rhodopsin: A G Protein-Coupled Receptor. *Science* **289**: 739-745.

Parthier C, Kleinschmidt M, Neumann P, Rudolph R, Manhart S, Schlenzig D, Fanghanel J, Rahfeld J U, Demuth H U and Stubbs M T (2007) Crystal Structure of the Incretin-Bound Extracellular Domain of a G Protein-Coupled Receptor. *Proc Natl Acad Sci U S A* **104**: 13942-13947.

Pioszak AA and Xu H E (2008) Molecular Recognition of Parathyroid Hormone by Its G Protein-Coupled Receptor. *Proc Natl Acad Sci U S A* **105**: 5034-5039.

Runge S, Thogersen H, Madsen K, Lau J and Rudolph R (2008) Crystal Structure of the Ligand-Bound Glucagon-Like Peptide-1 Receptor Extracellular Domain. *J Biol Chem* **283**: 11340-11347.

Salomon Y, Londos C and Rodbell M (1974) A Highly Sensitive Adenylate Cyclase Assay. *Anal Biochem* **58**: 541-548.

Schwartz TW, Frimurer T M, Holst B, Rosenkilde M M and Elling C E (2006) Molecular Mechanism of 7TM Receptor Activation--a Global Toggle Switch Model. *Annu Rev Pharmacol Toxicol* **46**: 481-519.

Solano RM, Langer I, Perret J, Vertongen P, Juarranz M G, Robberecht P and Waelbroeck M (2001) Two Basic Residues of the H-VPAC1 Receptor Second Transmembrane Helix Are Essential for Ligand Binding and Signal Transduction. *J Biol Chem* **276**: 1084-1088.

Sun C, Song D, Davis-Taber R A, Barrett L W, Scott V E, Richardson P L, Pereda-Lopez A, Uchic M E, Solomon L R, Lake M R, Walter K A, Hajduk P J and Olejniczak E T (2007) Solution Structure and Mutational Analysis of Pituitary Adenylate Cyclase-Activating Polypeptide Binding to the Extracellular Domain of PAC1-RS. *Proc Natl Acad Sci U S A* **104**: 7875-7880.

Vilardaga JP, Frank M, Krasel C, Dees C, Nissenson R A and Lohse M J (2001) Differential Conformational Requirements for Activation of G Proteins and the Regulatory Proteins Arrestin and G Protein-Coupled Receptor Kinase in the G Protein-Coupled Receptor for Parathyroid Hormone (PTH)/PTH-Related Protein. *J Biol Chem* **276**: 33435-33443.

Warne T, Serrano-Vega M J, Baker J G, Moukhametzianov R, Edwards P C, Henderson R, Leslie A G, Tate C G and Schertler G F (2008) Structure of a Beta1-Adrenergic G-Protein-Coupled Receptor. *Nature* **454**: 486-491.

This article has not been copyedited and formatted. The final version may differ from this version.   26

FOOTNOTES

LEGENDS FOR FIGURES

Figure 1: Alignment used to produce the VPAC$_1$ receptor model (finalAln). Neither the N-terminal nor the C-terminal parts of the template (bovine visual rhosopsin, OPSD) and target (VPAC$_1$) are shown, although loop regions are presented. All gaps were imposed to be approximately in the middle of loops. TM segments (experimentally resolved for rhodopsin and predicted from UniProt data for VPAC$_1$) are grey-highlighted. Residues that were mutated in this work are underlined. The most conserved residues in TM segments of family A and B receptors are in bold on OPSD and VPAC$_1$ sequences, respectively. A single residue per helix is given for rhodopsin — the one that is used as an "anchor" point in well-known Ballesteros-Weinstein GPCR-A numbering system (Ballesteros and Weinstein, 2005). The conserved residues in TM helices of VPAC$_1$ receptor may serve as a "signature" for automated identification of family B GPCRs from the sequence (Bissantz *et al.*, 2004). Notice that virtually none of such residues coincide in both families. The average calculated degree of sequence identity of TM helices on the alignment is about 10%, which is at the lower boundary of the so-called "twilight zone" in comparative modelling (Baker and Sali, 2001). Other alignment variants that where used for construction of the "final" (this one) are shown in Fig. S1 in Supplementary Material.

Figure 2: Schematic view of the packing quality of VPAC$_1$ models built from different alignments. The curves represent distributions of the membrane score values (S^{mem}) — each for an ensemble of 1000 MD conformers with fixed C$_\alpha$ atoms positions. Thick solid lines correspond to distributions obtained from the ReAln alignment (grey) and the manually corrected version finalAln (black). Arrows of the same colors show S^{mem} values for the starting conformations, before MD sampling. Broken lines correspond to models built using the four initial alignments Aln-1–4 (See Fig. S1 in Supplementary Material). Notice that the finalAln model, initially worse packed than the ReAln model, becomes superior in terms of the $<S^{mem}>$ value of the MD derived distribution. This suggests that the backbone of the finalAln model permits more advantageous conformations and environments for side chains, and therefore this model should be considered as better packed.

Figure 3: 3D model of the TM domain of VPAC$_1$ receptor. Each of the TM α-helices is individually colored and marked. The most important residues that are discussed in the main text are shown including R^{188}, N^{229} and Q^{380} that were mutated in this study. (A) Side view (from the membrane). (B) Top view (from the extracellular space). (C) Zoomed view of the mutated region (the view direction is shown by the orange arrow in *A*). Mutated residues form a chain: R^{188} in TM2–Q^{380} in TM7–N^{229} in TM3.They possibly form hydrogen bonds, as shown with dashed orange lines. Note that the figure illustrates the possibility of forming H-bonds but does not imply that two these interactions should (or may) exist simultaneously.

Figure 4: Binding and adenylate cyclase assay of wt and mutated VPAC$_1$. Left panel: Inhibition of [^{125}I]-VIP binding to membranes from CHO cells expressing the wt or the mutated VPAC$_1$ receptors by increasing concentrations of VIP. Right panel: Adenylate cyclase stimulation by VIP of the same membranes used in the left panel. The pIC$_{50}$ and pEC$_{50}$ and efficacy values, averaged over three experiments, are given in Table 1, along with the standard error.

Table 1: Effect of mutation of R^{188}, N^{229} and Q^{380} in human $VPAC_1$

a) Single mutants

	Binding studies			Adenylate cyclase assay		
	pIC_{50}	$\Delta\,pIC_{50}$	Receptor density (pmol/mg prot)	pEC_{50}	$\Delta\,pEC_{50}$	Emax (pmol/mg prot.min)
$VPAC_1$	8.53 ± 0.07		2.1 ± 0.2	8.59 ± 0.09		160 ± 3
$R^{188}A$ [a]	nd	-	-	-	-	-
$R^{188}N$	7.08 ± 0.07*	-1.45	2.0 ± 0.3	7.63 ± 0.11*	-0.96	140 ± 5
$R^{188}Q$ [a]	6.52 ± 0.05*	-2.01	1.9 ± 0.2	7.72 ± 0.06*	-0.87	152 ± 3
$N^{229}A$ [b]	8.42 ± 0.08	-0.11	2.3 ± 0.4	7.36 ± 0.11*	-1.23	50 ± 4*
$N^{229}Q$ [b]	8.57 ± 0.10	0.04	2.2 ± 0.3	7.58 ± 0.16*	-1.01	111 ± 9*
$N^{229}R$	8.65 ± 0.06	0.12	2.0 ± 0.3	8.48 ± 0.12	-0.11	123 ± 3*
$Q^{380}A$	8.61 ± 0.08	0.08	1.9 ± 0.2	7.30 ± 0.10*	-1.29	51 ± 4*
$Q^{380}N$	8.34 ± 0.08	-0.19	2.3 ± 0.3	8.35 ± 0.09	-0.20	106 ± 3*
$Q^{380}R$	7.18 ± 0.09*	-1.35	2.4 ± 0.2	7.81 ± 0.12*	-0.78	43 ± 3*

b) Double mutants

	Binding studies				Adenylate cyclase assay			
	pIC_{50}	$\Delta\,pIC_{50}$	Expected $\Delta\,pIC_{50}$	Receptor density (pmol/mg prot)	pEC_{50}	$\Delta\,pEC_{50}$	Expected $\Delta\,pIC_{50}$	Emax (pmol/mg prot.min)
$VPAC_1$	8.53 ± 0.07			2.1 ± 0.2	8.59 ± 0.09			160 ± 3
$N^{229}A/Q^{380}A$	7.61 ± 0.09*	-0.92	-0.03	2.0 ± 0.3	7.14 ± 0.13*	-1.45	-2.52	35 ± 5*
$R^{188}N/N^{229}R$	nd	-	-1.33	-	6.61 ± 0.12*	-1.98	-1.07	120 ± 4*
$R^{188}Q/Q^{380}R$	6.46 ± 0.04*	-2.07	-3.36	1.8 ± 0.3	6.41 ± 0.12*	-2.18	-1.65	35 ± 2*
$N^{229}Q/Q^{380}N$	7.87 ± 0.08*	-0.66	-0.15	2.3 ± 0.2	8.08 ± 0.11	-0.51	-1.21	117 ± 3*

pIC_{50} of binding, pEC_{50} and Emax of adenylate cyclase activation for VIP on membranes from CHO cells expressing the wild type $VPAC_1$ or mutated receptor. ΔpEC_{50} is defined as pEC_{50}(mutant)-pEC_{50}(wt) and ΔpIC_{50} as pIC_{50}(mutant)-pIC_{50}(wt). The expected values are the changes that would be expected if there was strict additivity. Emax is measured in response to 1 μM VIP and values represent the mean ± SEM of at least three independent experiments. *

Molecular Pharmacology Fast Forward. Published on June 23, 2010 as DOI: 10.1124/mol.110.063578

MOL #63578 This article has not been copyedited and formatted. The final version may differ from this version.   30

$p < 0.05$ evaluated by Mann-Whitney test. nd = not detectable. [a] from (Solano *et al.*, 2001) and [b] from (Nachtergael *et al.*, 2006).

Figure 1


```
TM1 OPSD   (35): WQFSMLAAYMFLLIMLGFPINFLTLYVTVQHKKLR 69
    VPAC1 (141): SVKTGYTIGYGLSLATLLVATAILSLFRKLHC--- 172

TM2 OPSD:      TPLNYILLNLAVADLFMVFGGFTTTLYTSLHGY-- 102
    VPAC1:    -TRNYIHMHLFISFILRAAAVFIKDLALFDSGESD 206

TM3 OPSD:     -FVFGPTGCNLEGFFATLGGEIALWSLVVLAIERYVVVCKPM 143
    VPAC1:     QCSEGSVGCKAAMVFFQYCVMANFFWLLVEGLYLYTLLAV-- 246

TM4 OPSD:      SNRFRGENHAIMGVAFTWVMALACAAPPLVGWSRYIPEGMQCSCG 188
    VPAC1:     -SFFSERKYFWGYILIGWGVPSTFTMVWTIARIHFEDYG------ 284

TM5 OPSD:      IDYYTPHEETNNESFVIYMFVVHFIIPLIVIFFCYGQLVFTVKEA- 233
    VPAC1:     --------CWDTINSSLWWIIKGPILTSILVNFILFICIIRILLQK 322

TM6 OPSD:      AAQQQESATTQKAEKEVTRMVIIMVIAFLICWLPYAGVAFYIFTH 278
    VPAC1:     LRPPDIRKSDSSPYSRLARSTLLLIPLFGVHYIMFAFFPDNF--- 364

TM7 OPSD:      QGSDFGPIFMTIPAFFAKTSAVYNPVIYIMMNKQFRNCMVTTLCCGK 325
    VPAC1:     ----KPEVKMVFELVVGSFQGFVVAILYCFLNGEVQAELRRKWRRW- 406
```
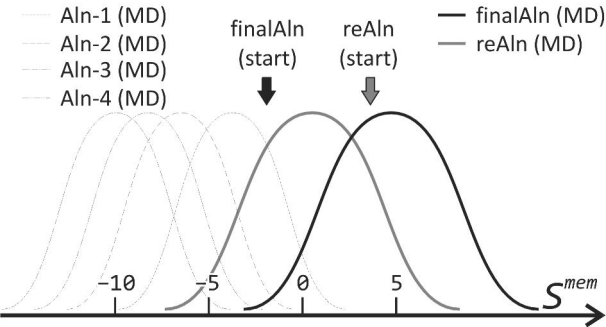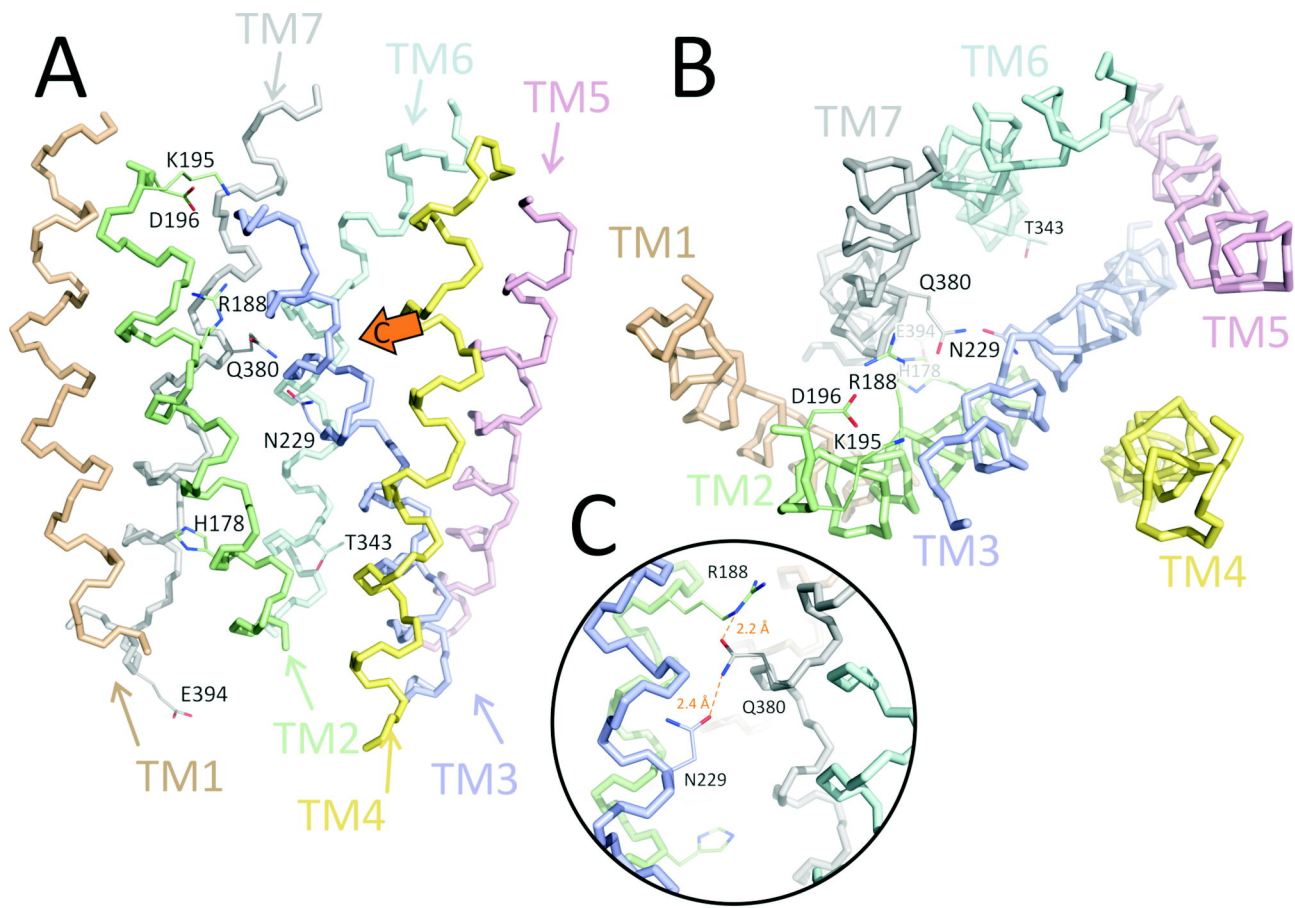
Figure 2

Figure 3

Figure 4